HADRONIC TRANSPORT MODELS*

P. Danielewicz

National Superconducting Cyclotron Laboratory and
Department of Physics and Astronomy, Michigan State University
East Lansing, MI 48824, USA
and Gesellschaft für Schwerionenforschung mbH
64291 Darmstadt, Germany

Hadronic transport models may be utilized to extract bulk nuclear properties. Deduction of in-medium nucleon–nucleon cross sections and of nuclear viscosity is discussed, as well as the extraction of momentum dependence of nucleonic mean field. Moreover, determination of the nuclear incompressibility and of constraints on the nuclear pressure at supranormal densities is described.

PACS numbers: 25.70.–z, 25.75.–q, 25.75.Ld, 25.70.Ef

1. Introduction

Hadronic transport is essential means for understanding energetic central reactions and for deducing properties of excited matter. The transport is generally based on the Boltzmann equation for the particle phase-space distributions f:

$$\frac{\partial f}{\partial t} + \frac{\partial \varepsilon_{\boldsymbol{p}}}{\partial \boldsymbol{p}} \frac{\partial f}{\partial \boldsymbol{r}} - \frac{\partial \varepsilon_{\boldsymbol{p}}}{\partial \boldsymbol{r}} \frac{\partial f}{\partial \boldsymbol{p}} = \int d\boldsymbol{p}_2 \int d\Omega' \, v_{12} \frac{d\sigma}{d\Omega'} \left((1-f_1)(1-f_2) \right.$$
$$\left. \times f_1' \, f_2' - (1-f_1')(1-f_2')f_1 \, f_2 \right). \tag{1}$$

Here, $\varepsilon(\boldsymbol{p}, \{f\})$ is the single particle energy. The terms on the l.h.s. of the equation account for the changes of f due to the motion of particles in the average potential field produced by other particles; the particle velocity is $\boldsymbol{v} = \partial \varepsilon / \partial \boldsymbol{p}$. The r.h.s. of (1) accounts for changes of f due to collisions.

The hadronic transport has been quite successful in applications, describing a multitude of measured single-particle spectra, among other. With

---

* Presented at the XXVII Mazurian Lakes School of Physics, Krzyże, Poland, September 2–9, 2001.

a confidence stemming from the success of predictions, one can gain through the transport theory a good insight into the history and mechanism of reactions. The transport theory is fairly flexible allowing one to include new particles as energy domain changes and to incorporate new collision processes if these become important.

Despite successes of the theory, there are significant uncertainties in the underlying Boltzmann equation. Thus, the dependence of the single-particle energies on momentum and density is generally not known. In terms of the net system energy, the single-particle energies are:

$$\varepsilon = \frac{\delta E}{\delta f}, \tag{2}$$

and they relate to particle optical potentials with

$$U_{\mathrm{opt}} = \varepsilon - \varepsilon_{\mathrm{kin}}. \tag{3}$$

The cross sections utilized in the collision integral in (1) are usually such as in free-space, but different cross sections may need to be utilized in the medium.

The indicated uncertainties represent difficulties but also opportunities to learn about nuclear systems. In practice, it is necessary to identify observables from reactions, or combinations thereof, that are sensitive to a specific uncertainty. It is necessary to understand which particular features of the nuclear system are explored in a reaction and why an outcome may be well described in spite of the uncertainties. In the following, I shall give examples of the inference of bulk properties of nuclear matter from comparing the transport results to reaction data, emphasizing the above points.

2. Stopping in collisions

Stopping observables in collisions, such as linear momentum transfer and $ERAT$, can be expected to yield information on in-medium cross-sections. In the linear-momentum measurements, central ($b \sim 0$) mass asymmetric reactions are assessed within the laboratory frame, *cf.* Fig. 1. The velocity
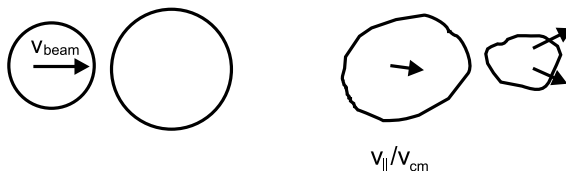

Fig. 1. A mass-asymmetric collision.

component along the beam of the most massive fragment stemming from a reaction is identified, and its average over reaction events is compared to the c.m. velocity. A proximity of the average component to the net c.m. velocity, $\langle v_\parallel \rangle \sim v_{\rm c.m.}$, indicates fusion in a reaction and, thus, a large level of stopping and, potentially, large elementary cross sections. On the other hand, low values of the average component, $\langle v_\parallel \rangle \sim 0$, indicate little stopping and, potentially, low elementary cross sections.

The Stony Brook group [1] has investigated central ($\langle b \rangle \sim b_{\rm max}/4$) collision events of Ar with several targets, Cu, Ag and Au, and has determined $\langle v_\parallel \rangle / v_{\rm c.m.}$ as a function of bombarding energy; the results from the Ag target are represented by filled circles in Fig. 2. At low energies, the projectile
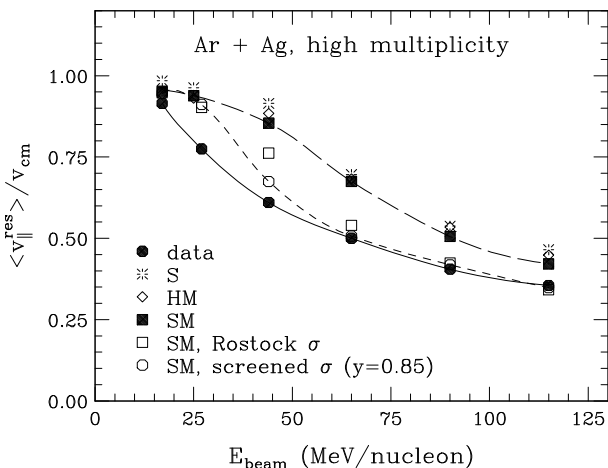

Fig. 2. Measured (filled circles) and calculated (other symbols) average velocity ratio $\langle v_\parallel \rangle / v_{\rm c.m.}$ as a function of beam energy in central ^{40}Ar + Ag collisions.

and target appear to fuse. As energy is raised, the transparency sets in and it increases with the increase in energy. Results of transport simulations assuming free nucleon–nucleon cross sections and different forms of optical potentials are represented, respectively, by stars, diamonds and filled squares in the figure. It is seen that all those calculations overestimate the stopping. The fusion continues too high up in energy and at high energies the residue velocity remains too high. Notably, the results are rather incentive to the assumed form of nucleon single-particle energies. In consequence, these results point to the in-medium cross-sections reduced compared the free-space.

There may be different reasons for an in-medium reduction of cross sections. Thus, it may be reasonable to assume that the geometric cross-section radius should not exceed the interparticle distance,

$$\sigma \lesssim y\,\rho^{-2/3}\,, \tag{4}$$

with $y \sim 1$, since, otherwise, the nucleon–nucleon scatterings can get multiply counted. The requirement may be implemented in practice with the following in-medium cross section:

$$\sigma = \sigma_0 \, \tanh\left(\sigma_{\mathrm{free}}/\sigma_0\right), \qquad \text{where} \qquad \sigma_0 = y \, \rho^{-2/3}. \qquad (5)$$

There may be other reasons for the cross-section reduction, such as the effects of Pauli principle and of single-particle energy modifications for intermediate states. In the calculations that include those effects (but not the overlap of binary collision regions), such as of the Rostock group [2], a general reduction of the in-medium cross sections is found. In the following, we utilize a crude parametrization of the Rostock cross sections:

$$\sigma = \sigma_{\mathrm{free}} \, \exp\left(-0.6 \, \frac{\rho}{\rho_0} \, \frac{1}{1 + (T_{\mathrm{c.m.}}/150\,\mathrm{MeV})^2} \right), \qquad (6)$$

where $T_{\mathrm{c.m.}}$ is the c.m. kinetic energy of a scattering nucleon pair.

The results of the simulations using the two types of reduced in-medium cross-sections are shown in Fig. 2 with open squares and open circles, respectively. It is seen that the stopping is reduced now at higher energies and in a much better agreement with data.

While similar reductions are obtained with the two in-medium cross sections, the two cross sections are actually quite different. This is illustrated in Fig. 3 that shows the number of collisions for the different cross sections, as a function of time. It is seen that the number of collisions for the Rostock cross sections is reduced by $\sim 25\%$ compared to the free cross-sections. However, the number of collisions for the cross sections screened with the interparticle distance is reduced by a factor of 4. How come those two cross sections lead to the same reduction in stopping when the collision numbers are so vastly different?

Clearly, not all collisions are the same. If *e.g.* the scattering angle in collision is small, the collision may matter little for the reaction dynamics. The most elementary macroscopic property of a system related to the cross sections is viscosity. When a system is described by the Boltzmann equation, then the viscosity is [3]

$$\eta = \frac{\frac{5}{9}\, T \, \left[\int d\boldsymbol{p}\, p^2 \, f\right]^2}{\int d\boldsymbol{p}_1 \int d\boldsymbol{p}_2 \int d\Omega' \, v_{12} \frac{d\sigma}{d\Omega'} \, q_{12}^4 \sin^2 \theta'} \, f_1 \, f_2 \, (1 - f_1')\,(1 - f_2'), \qquad (7)$$

where the relative momentum is $q_{12} = |\boldsymbol{p}_1 - \boldsymbol{p}_2|/2$. The viscosity is inversely proportional to the binary collision rate, but with collisions weighted with the weight $q_{12}^4 \sin^2 \theta'$, suppressing the collisions at low scattering angle, and weighting most those that take place at large relative momentum and lead to $\theta' \, 90°$.
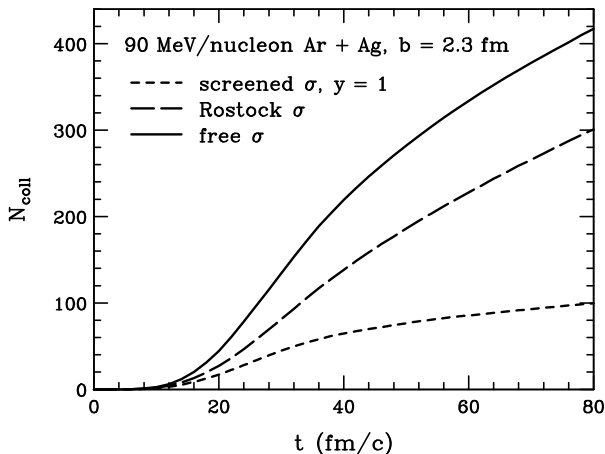
Fig. 3. Number of collisions in the 90 MeV/nucleon Ar + Ag reaction for different cross sections, as a function of time.

While the two different parametrizations of cross sections yield different results regarding the collision number, it is interesting to ask whether they also yield different results for collisions weighted with their importance, such as in the expression for viscosity. This is examined in Fig. 4 and it is seen that the two parametrizations, that yield a right reduction in stopping, also practically agree with regard to the weighted collision number. These parametrizations would also agree with regard to the viscosity of the system, increased by the same factor by which the weighted collision number is decreased.
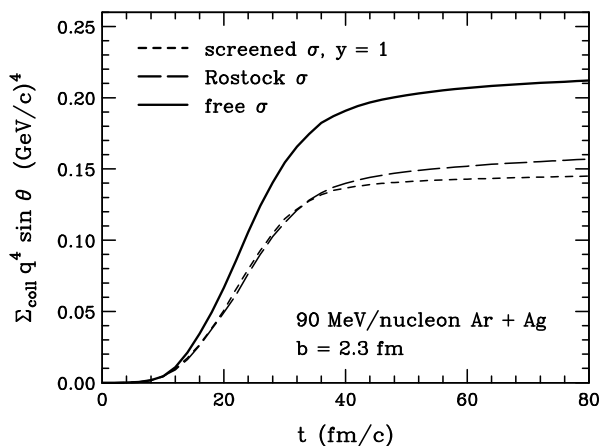

Fig. 4. Number of collisions weighted with $q^4 \sin^2 \theta$ in the 90 MeV/nucleon Ar + Ag reaction for different cross sections, as a function of time.

Another nuclear stopping observable has been the reaction cross section for different values of $ERAT = E_\perp/E_\parallel$, examined in central Au + Au collisions by the FOPI Collaboration [4]. Here, $E_\perp$ and $E_\parallel$ are the transverse and longitudinal energy, respectively. Generally, a value of $ERAT < 2$ indicates a transparency (2 because of two transverse dimensions and only one longitudinal), $ERAT > 2$ indicates a system splashing in the directions transverse to the beam axis, and $ERAT = 2$ indicates isotropy. However, finite-multiplicity fluctuations spread out and modify those results and likewise do the detector inefficiencies. After correcting for the fluctuations and inefficiencies, the FOPI Collaboration concluded that the head-on Au + Au collisions at 250 MeV/nucleon were consistent with isotropy. Figure 5 shows the results for the expected value of $ERAT$ in simulations, with the variation of the inverse of parameter y in the first of our in-medium cross-section parametrization, together with the result for the second parametrization and for data (with 10% uncertainty). The value of $1/y = 0$ corresponds to free cross sections and these again yield too much stopping. The compatibility with data requires $y \sim 1$. In the analysis, the Rostock and screened cross-section parametrizations yield again very different collision numbers, but similar numbers for collisions entered with viscous weight, when those parametrizations yield a similar stopping. The number of weighted collisions is again reduced by about 25% compared to the case of free cross sections.
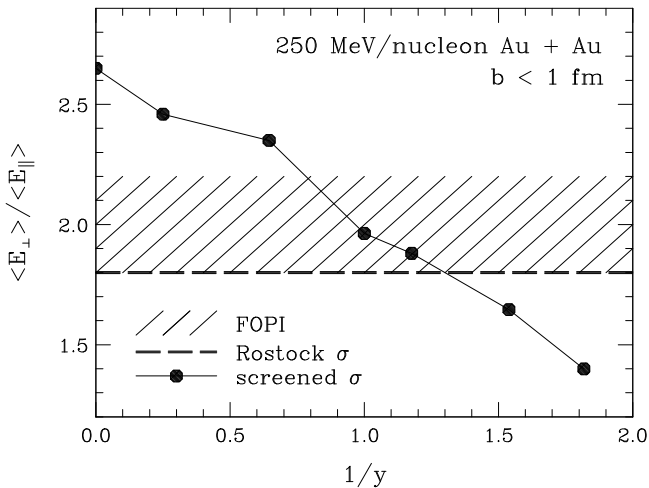

Fig. 5. $ERAT$ in central Au + Au reactions at 250 MeV/nucleon. The filled circles represent the results of simulations as a function of the parameter $1/y$ controlling the cross section reduction in (5). The dashed line represents the result of simulations with Rostock cross sections (6). The dashed region represents the data of Ref. [4].

Based on the simulations, we can conclude that the stopping observables indicate reduced in-medium cross sections and that these observables directly sense the nuclear viscosity. In the reactions in question, the viscosity is higher by $\sim 25\%$ compared to that expected on the basis of free cross sections [3].

3. Mean-field momentum dependence

Elastic scattering of nucleons from nuclei and nuclear structure give access to the nucleonic mean fields (MFs) at densities $\rho \lesssim \rho_0$ and yield evidence for nontrivial momentum dependence of those fields, see Fig. 6. However, it had been difficult to demonstrate the momentum dependence of the fields in heavy-ion collisions and, in particular, to access the momentum dependence at supranormal densities reached in the collisions.
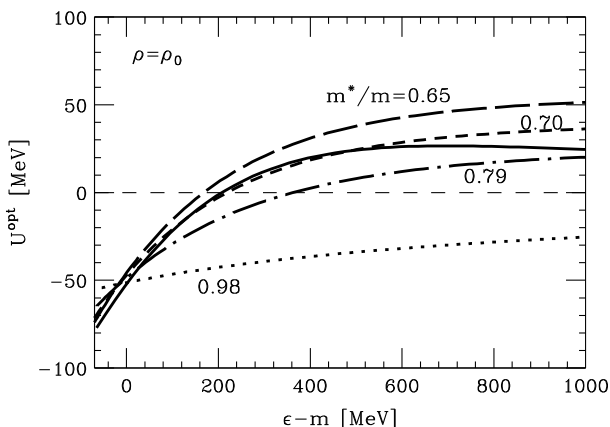

Fig. 6. Nucleon mean field in symmetric matter at ρ_0 as a function of nucleon momentum. Solid line represents parametrization [5] of data analyses, in particular from nucleon scattering by Hama *et al.* [6]. Other lines represent different MF parametrizations in simulations.

In Fig. 6, we see that the optical potential is an increasing function of the momentum. The expected effect of the momentum dependence of the field in a reaction is then an increase in the particle velocity in the medium, as

$$v = \frac{\partial \varepsilon}{\partial p} \frac{\partial \varepsilon^{\mathrm{kin}}}{\partial p} + \frac{\partial U^{\mathrm{opt}}}{\partial p} = v^{\mathrm{kin}} + \frac{\partial U^{\mathrm{opt}}}{\partial p} > v^{\mathrm{kin}}, \tag{8}$$

cf. (3), where v^{kin} is velocity in free space for a given p. One measure of the momentum dependence is the effective mass m^*, the ratio of the momentum to the velocity, usually considered at the Fermi surface. A stronger momentum dependence yields a lower m^*.

In simulations, it is convenient to parametrize in-medium particle velocities in a local frame and to derive single-particle energies and potentials therefrom, with [7]

$$v(p, \rho) \;=\; \frac{p}{\sqrt{p^2 + m^2 \left/ \left(1 + c\,\frac{\rho}{\rho_0}\,\frac{1}{(1 + \lambda\,p^2/m^2)^2}\right)^2\right.}} \,, \tag{9}$$

$$\varepsilon(p, \rho) \;=\; m + \int_0^p dp'\, v + \Delta\varepsilon(\rho) \,. \tag{10}$$

This precludes supraluminous behavior.

The question arises how to demonstrate a change in the particle velocities in a reaction. One possibility is to use a timer represented by the spectator nucleons in the periphery of a reaction. Figure 7 shows contour plots of the baryon density, excitation energy, and of the bound baryons in an 800 MeV/nucleon Sn + Sn reaction at $b = 5$ fm. The spectator nucleons,
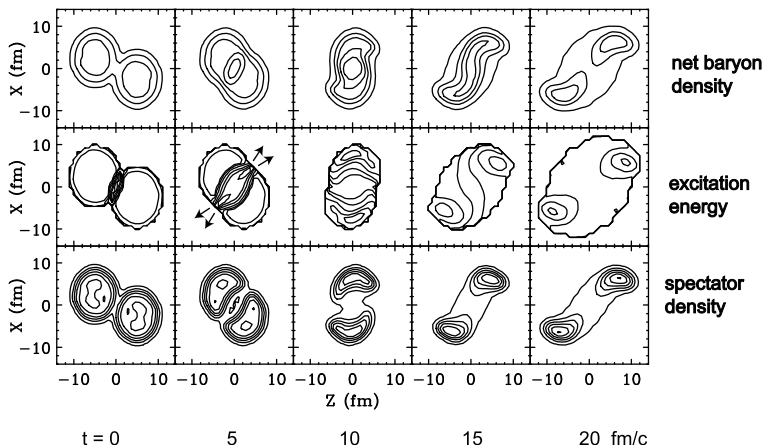

Fig. 7. Contour plots of baryon density, excitation energy and of density of bound baryons in the ^{124}Sn + ^{124}Sn reaction at 800 MeV/nucleon [7].

at the edges of the system, are only weakly affected by the reaction process and proceed at a virtually unchanged velocity. At the same time, the so-called participant particles at the center of the system undergo collisions with particles from the opposing nucleus. The participant region undergoes compression and excitation followed by expansion. Of interest are velocities of particles in the compressed region and those velocities can be assessed through anisotropies due the shadow of spectator matter in the emission of high momentum particles leaving the participant region. Given the fixed

velocity of the spectators, the shadow and emission anisotropy will be pronounced if the participant particles are fast and weak if the participants are slow.

The spectator pieces are large in more peripheral collisions and there also the importance of the MF momentum dependence is pronounced as the matter does not equilibrate well. The anisotropy of particle emission at midrapidity (zero longitudinal velocity in the c.m.), quantified in terms of a so-called ellipticity coefficient $v_2 = \langle \cos(2\phi) \rangle$, is shown in Fig. 8 for the Au + Au collision at 400 MeV/nucleon, as a function of the impact parameter. It is apparent that at high b it is possible to separate the effects of MFs with and without the momentum dependence and even possibly to learn about details of the momentum dependence.
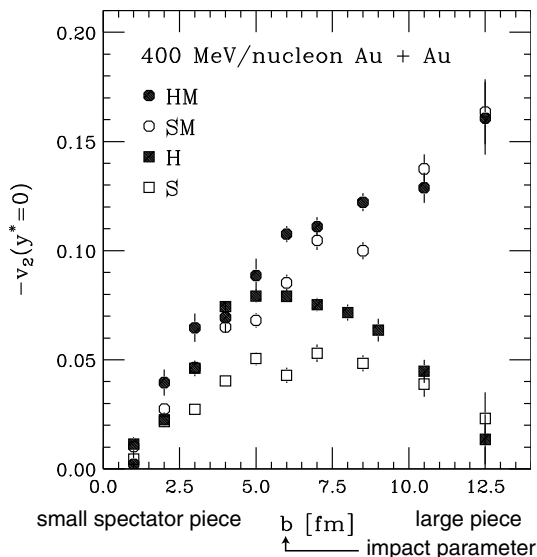

Fig. 8. Negative of the ellipticity parameter at midrapidity in Au + Au collisions at 400 MeV/nucleon, as a function of the impact parameter [6]. The circles represent results for momentum-dependent MFs characterized by $m^* = 0.65m$ and different incompressibilities, while squares represent results for momentum-independent MFs (characterized by $m^* = m$).

The anisotropy of proton emission at midrapidity has been studied by the KaoS Collaboration [8] in midperipheral Bi+Bi collisions as a function of proton transverse momentum, at several beam energies. Their 400 MeV/nucleon results, in terms of the out-of to in-plane anisotropy

$$R_N = \frac{N(90°) + N(270°)}{N(0°) + N(180°)} = \frac{1 - 2v_2}{1 + 2v_2}, \tag{11}$$

are compared in the top panel of Fig. 9 to the calculations utilizing MFs with
different momentum dependencies. It is apparent that the high-momentum
data favor the momentum-dependence characterized by the effective mass
in the vicinity of $m^* = 0.70m$.

The question is whether the conclusions on the momentum dependence
strongly depend on other uncertainties, such as the incompressibility or the
in-medium cross sections. This is tested in the bottom panel of Fig. 9. It
is seen that sensitivity of the R_N in midperipheral collisions to the other
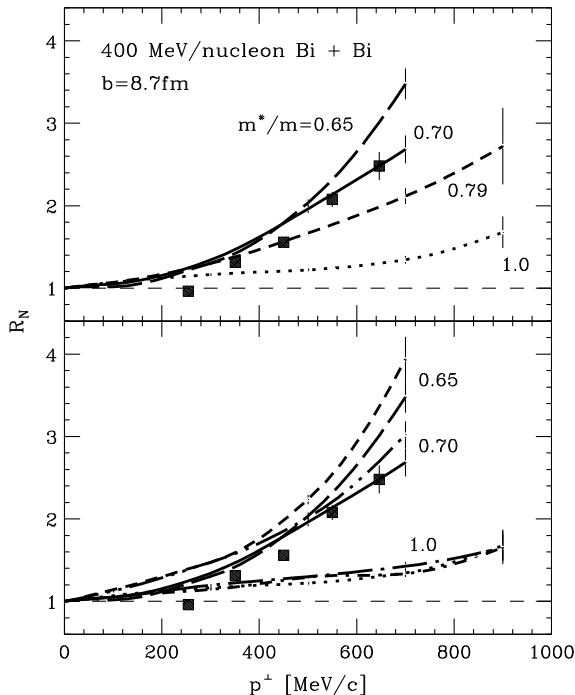uncertainties is weak.

Fig. 9. Measured [8] (filled squares) and calculated [6] (lines) ratios R_N, as a func-
tion of transverse momentum, in Bi + Bi reaction. The lines in the top panel
represent the results of simulations with in-medium cross sections and those MFs
for which the optical potentials are shown in Fig. 6. The bottom panel shows the
sensitivity of the results to the variation of cross sections and of K. The long-
dashed, solid, and dotted lines repeat respective results from the top panel ob-
tained with in-medium cross sections and $K = 210$ MeV. The long-dash-dotted
and short-dash-dotted lines represent additional results obtained, respectively, us-
ing the momentum-independent MF with $K = 380$ MeV and using no MF at all.
The short-dashed and long-dash-double-dotted lines represent the additional results
for free cross-sections and MFs with $m^*/m = 0.65$ and $m^*/m = 0.70$, respectively.

Another question that arises is whether the reactions in question provide the same information that can be gained from nucleon–nucleus scattering or whether new information is gained pertaining to supranormal densities. To test this, simulations may be carried out by varying the momentum dependence at supranormal but not at lower densities. The bottom panel of Fig. 10 compares 700 MeV/nucleon data [8] to the results of simulations assuming the momentum dependence given by (9), strengthening with the increase in density, and to the results of simulations assuming the same momentum dependence at supranormal densities as at the normal:

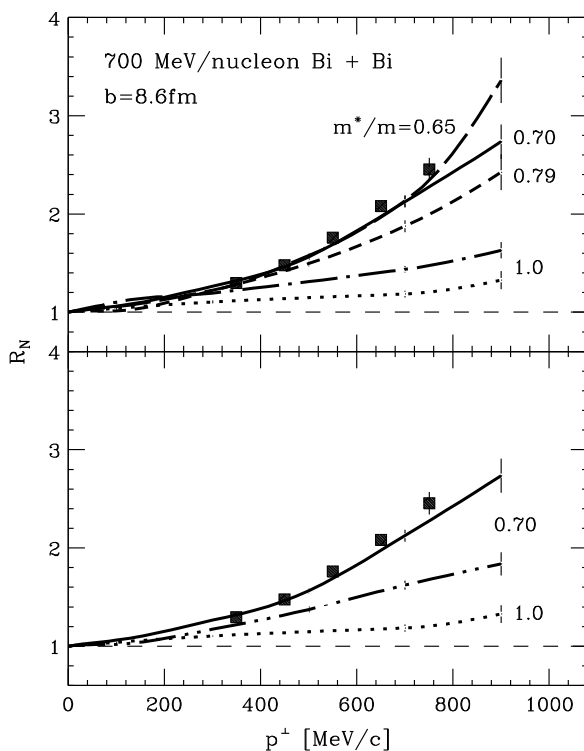$$v(p, \rho) = v(p, \rho_0), \qquad \text{for} \quad \rho > \rho_0 \,. \tag{12}$$

Fig. 10. Measured [8] (filled squares) and calculated [6] (lines) ratios of out-of-plane to in-plane proton yields at midrapidity, as a function of $p^\perp$, in 700 MeV/nucleon ^{209}Bi + ^{209}Bi collisions. The incompressibility is $K = 380$ MeV for the long-dash-dotted line in the top panel and $K = 210$ MeV for other calculations. The solid and dotted lines in the bottom panel repeat the results from the top panel. The long-dash-double-dotted line in the bottom panel represents the results of a calculation where the momentum dependence at $\rho > \rho_0$ is made to follow the dependence at $\rho = \rho_0$.

It is seen in the figure that the data clearly require the momentum dependence that strengthens with density; the results with the momentum dependence frozen above ρ_0 are in fact closer to those without the momentum dependence than those with the full dependence. The reason for the sensitivity to the momentum dependence at $\rho > \rho_0$ is that the high-$p^\perp$ particles are directly emitted into the vacuum from the high-density participant region around the time of maximum compression [6].

The parametrization of the momentum dependence that is favored by the data agrees fairly well with that found in the microscopic Dirac–Brueckner calculations [10,11] at the explored densities and momenta, see Fig. 11, but not with some other [6]. After tackling the in-medium cross-sections and the mean-field momentum dependence, we now turn to the features of the nuclear equation of state (EOS).
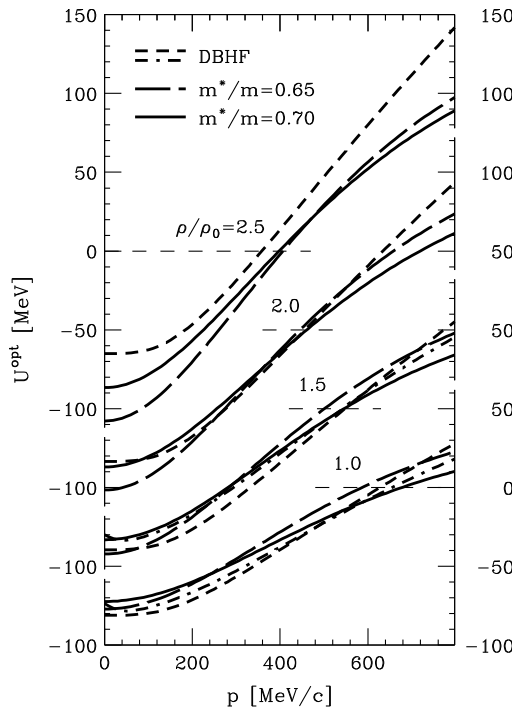

Fig. 11. Optical potential in nuclear matter as a function of nucleon momentum, at different densities, from the Dirac–Brueckner–Hartree–Fock (DBHF) calculations with the Bonn-A interaction and in our parametrizations. The short-dashed and short-dash-dotted lines represent the DBHF potentials obtained assuming, respectively, momentum-independent vector and scalar fields [10] and parametrized momentum-dependent fields [11] The solid and long-dashed lines represent the optical potentials for $m^*/m = 0.70$ and $m^*/m = 0.65$ MF parametrizations [6], respectively, with $K = 210$ MeV.

4. Nuclear incompressibility

From the binding-energy formula and from electron scattering, we know that the energy per nucleon in symmetric nuclear matter, under the effects of nuclear forces alone, minimizes at the normal density $\rho_0 = 0.16$ fm^{-3} at -16 MeV. The curvature around the minimum is quantified in terms of incompressibility K, first introduced as a curvature of the energy with respect to the nuclear radius for considered sharp-sphere nuclei,

$$K = 9\,\rho_0^2\,\frac{d^2}{d\rho^2}\left(\frac{E}{A}\right) = R^2\,\frac{d^2}{dR^2}\left(\frac{E}{A}\right)\,. \tag{13}$$

The simplest way to determine the incompressibility may seem to induce volume oscillations in a nucleus. This could be done by scattering α particles off a nucleus, Fig. 12. For the lowest excitation, the excitation energy E^*, deduced from the final α energy, would be related to the classical frequency through $E^* = \hbar\Omega$, and the latter would be related to K.
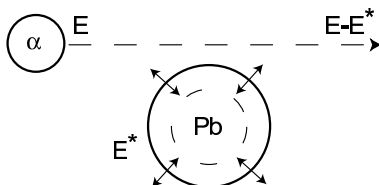

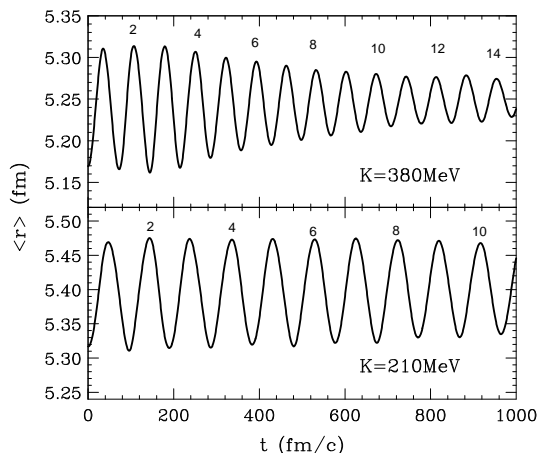Fig. 12. Volume oscillations induced by alpha scattering.

Fig. 13. Radius of an expanded lead nucleus as a function of time from the Vlasov version of (1), for two values of incompressibility.
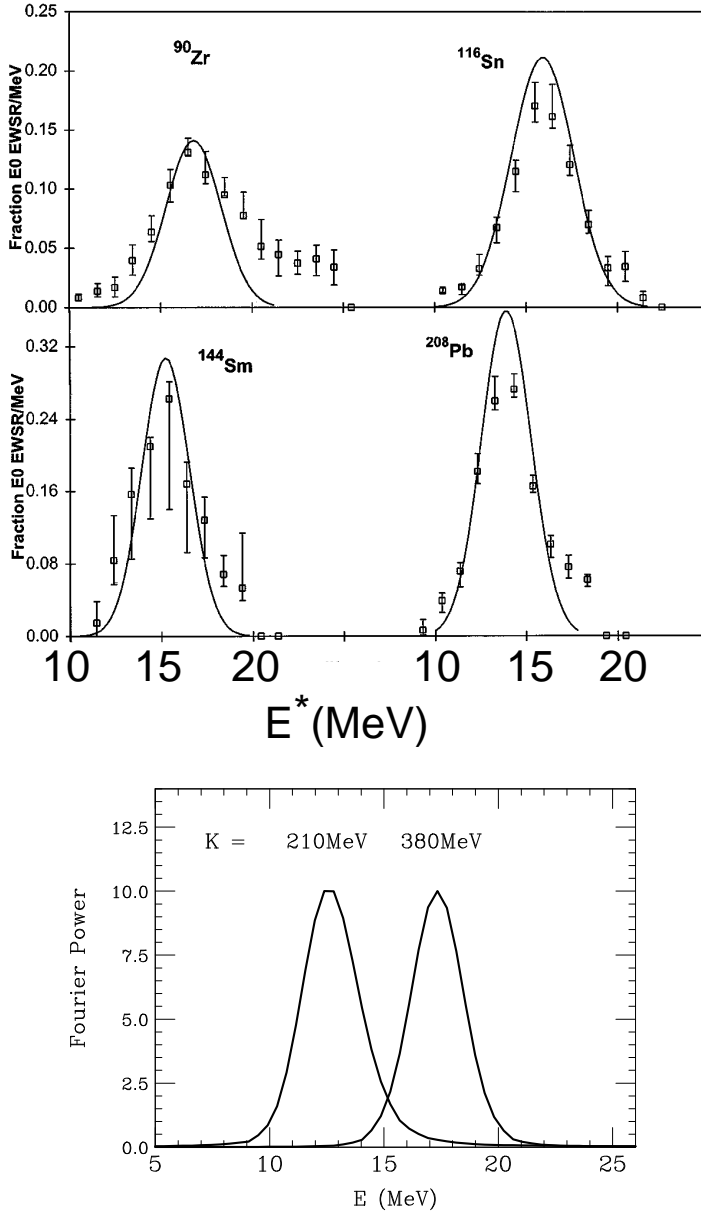
Fig. 14. Upper: 0^+ excitation spectrum in several nuclei from measurements of Youngblood *et al.* [13]. Lower: Fourier spectrum for monopole oscillations in lead within the Vlasov equation for two values of K.
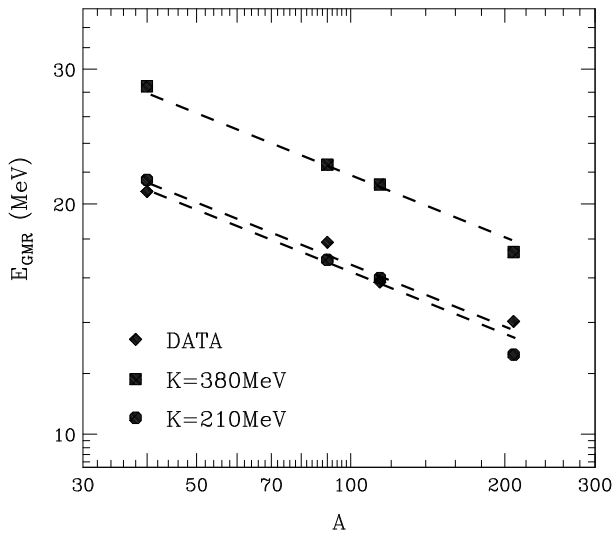
Fig. 15. Measured [13] and calculated energies of giant monopole resonances in spherical nuclei.

Let us examine the classical energy of an oscillating nucleus:

$$
\begin{aligned}
E_{\text{tot}} &= \int d\boldsymbol{r}\, \rho\, \frac{m_N\, v^2}{2} + \frac{1}{2}\, A\, K\, (R - R_0)^2 \\
&= \frac{A m_N \langle r^2 \rangle_A \dot{R}^2}{2} + \frac{1}{2}\, A\, K\, (R - R_0)^2\,,
\end{aligned}
\tag{14}
$$

where we use the fact that, for a nucleus uniformly changing its density, the velocity is proportional to the radius, $v = \dot{R}(r/R)$. We then obtain the energy of a simple harmonic oscillator; the frequency is a square root of the spring constant divided by mass constant, yielding:

$$
E^* = \hbar \sqrt{\frac{K}{m_N\, \langle r^2 \rangle_A}}\,.
\tag{15}
$$

There are complications regarding this reasoning. Thus, the nucleus is not a sharp-edged sphere and the Coulomb interactions play a role in the os-cillations as well as nuclear interactions, different in isospin asymmetric mat-ter than symmetric. These effects may be accounted for in time-dependent Hartree–Fock or in the random-phase-approximation calculations allowing for meaningful comparisons to data. The above approaches include also shell effects but, if one wants to study just average features of excitations, then the model based on (1) may be employed, provided that the net energy includes

contributions from the finite-range of interactions besides Coulomb, isospin and symmetric volume terms [6]. If a nucleus is expanded, by increasing distances from the center by a small fraction, then oscillations result, illustrated in Fig. 13, with a distinct dependence on K. Figure 14 shows next the power spectrum for the oscillations from the Boltzmann equation as well as the 0^+ spectra from precise analyses of alpha scattering [12], in the scattering angle and energy loss. Next, figure 15 compares the mass dependence of the resonance energy with the results from the Vlasov equation. The data favor $K = 225 \pm 15$ MeV, represented by the intermediate line.

5. EOS at supranormal densities from flow

Features of EOS at supranormal densities can be inferred from global features of flow in collisions of heavy nuclei at high energies. At low impact parameters, relatively large regions of high density are formed and matter is best equilibrated. The collective flow can provide access to pressure generated in the collision.

To see how the flow relates to pressure, we may look at the hydrodynamic Euler equation for the nuclear fluid, an analog of the Newton equation, in a local frame where the collective velocity vanishes, $v = 0$:

$$(e + p) \frac{\partial}{\partial t} \vec{v} = -\vec{\nabla} p. \tag{16}$$

The collective velocity becomes an observable at the end of the reaction. In comparing to the Newton equation, we see that the pressure $p = \rho^2 \frac{\partial(e/\rho)}{\partial \rho}|_{s/\rho}$ plays the role of a potential for the hydrodynamic motion, while the density of enthalpy $w = e + p$ plays the role of a mass. In fact, at moderate energies, the enthalpy density is practically the mass density, $w \approx \rho\, m_N$. We see from the Euler equation that the collective flow can tell us about the pressure in comparison to enthalpy. In establishing the relation, we need to know the spatial size where the pressure gradients develop and this will be determined by the nuclear size. However, we also need the time during the hydrodynamic motion develops and here again we will be able to use the spectators.

Notably, the first observable that one may want to consider to extract the information on EOS is the net radial or transverse collective energy. That energy may reach as much as half of the total kinetic energy in a reaction. Despite its magnitude, the energy is not useful for extracting the information on EOS because of the lack of information on how long the energy develops. Large pressures acting over a short time can produce the same net collective energy as low pressures acting over a long time.

However, the development of anisotropies in the collective expansion is timed by the spectators [14]. As the participant zone expands, the spectators, moving at a prescribed pace, shadow the expansion. If the pressures

in the central region are high and the expansion is rapid, the anisotropies generated by the presence of spectators are going to be strong. On the other hand, if the pressures are low and, correspondingly, the expansion of the matter is slow, the shadows left by spectators will not be very pronounced.

There are different types of anisotropies in the emission that the spectators can produce. Thus, throughout the early stages of a collisions, the particles move primarily along the beam axis in the center of mass. However, during the compression stage, the participants get locked within a channel, titled at an angle, between the spectator pieces, *cf.* Fig. 7. As a consequence, the forward and backward emitted particles acquire an average deflection away from the beam axis, towards the channel direction. Another anisotropy is the ellipticity v_2, that we already examined as a function of $p^\perp$ in midperipheral collisions. Now we will consider global v_2 values at lower impact parameters.

The different anisotropies have been quantified experimentally over a wide range of bombarding energies in Au + Au collisions. Figure 16 shows the measure of the sideward forward-backward deflection as a function of the beam energy, with symbols representing data. Lines represent simulations assuming different EOS. On top of the figure, typical maximal densities are indicated which are reached at a given bombarding energy. Without interaction contributions to pressure, the simulations labeled cascade produce far too weak anisotropies to be compatible with data. The simulations with EOS characterized by the incompressibility $K = 167$ MeV yield adequate anisotropy at lower beam energies, but too low at higher energies. On the other hand, with the EOS characterized by $K = 380$ MeV, the anisotropy appears too high at virtually all energies. It should be mentioned that the incompressibilities should be considered here as merely labels for the different utilized EOS. The pressures resulting in the expansion are produced at densities significantly higher than normal and, in fact, changing in the course of the reaction.

Figure 17 shows next the anisotropy of emission at midrapidity, with symbols representing data and lines representing simulations. Again, we see that without interaction contributions to pressure, simulations cannot reproduce the measurements. The simulations with $K = 167$ MeV give too little pressure at high energies, and those with $K = 380$ MeV generally too much. A level of discrepancy is seen between data from different experiments.

We see that no single EOS allows for a simultaneous description of both types of anisotropies at all energies. In particular, the $K = 210$ MeV EOS is the best for the sideward anisotropy, and the $K = 300$ MeV EOS is the best for the elliptic anisotropy. We can use the discrepancy between the conclusions drawn from the two types of anisotropies as a measure of inaccuracy of the theory and draw broad boundaries on pressure as a function
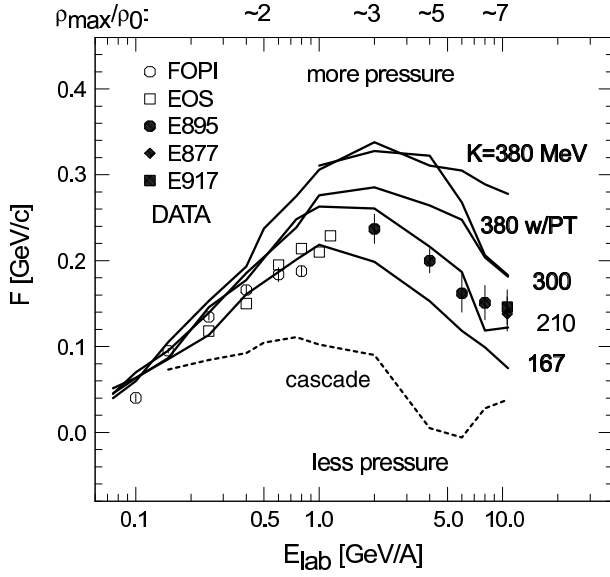
Fig. 16. Sideward flow excitation function for Au + Au. Data and transport calculations are represented, respectively, by symbols and lines [14].
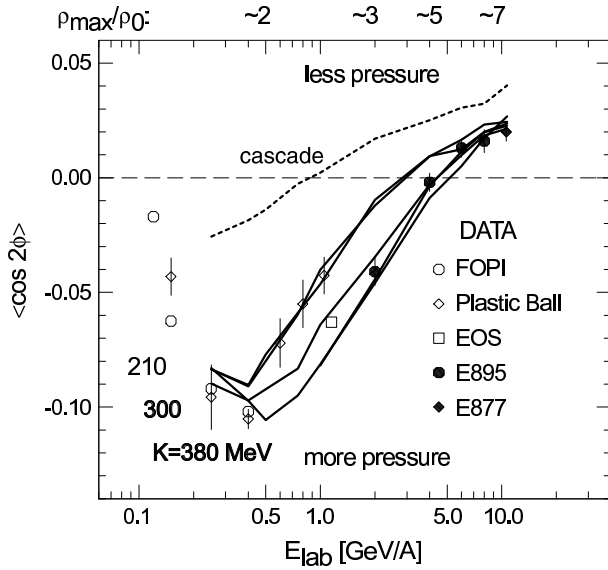

Fig. 17. Elliptic flow excitation function for Au + Au. Data and transport calculations are represented, respectively, by symbols and lines [14].

of density from what is common in conclusions based on the two anisotropies. To ensure that the effects of compression dominate in the reaction over other effects, we limit ourselves to densities higher than twice the normal. The boundaries on the pressure are shown in Fig. 18 and they eliminate some of the more extreme models for EOS utilized in nuclear physics, such as the relativistic NL3 model and models assuming a phase transition at relatively low densities, *cf.* Fig. 19.
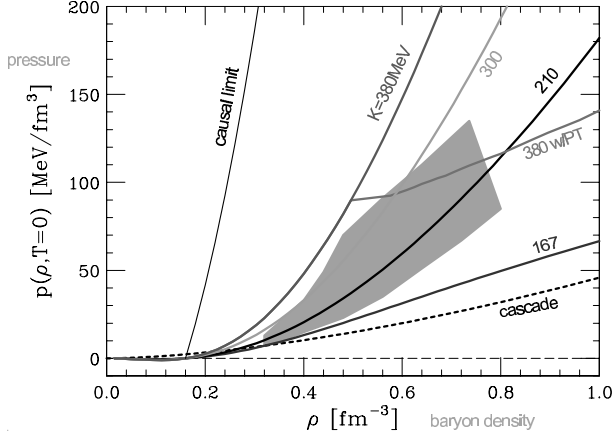
Fig. 18. Constraints from flow on the $T = 0$ pressure-density relation, indicated by the shaded region [14].
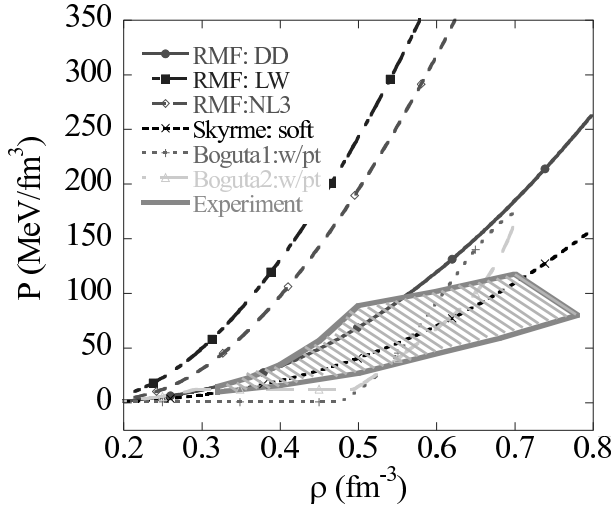
Fig. 19. Impact of the constraints on models for EOS [14].

6. Conclusions and outlook

Comparisons of transport model calculations to data can yield information on bulk nuclear properties. However, the progress has been difficult due to the need to sort out competing physical effects. Optimal observables are those which are mostly sensitive to one uncertain nuclear property.

Though the stopping observables are sensitive to the in-medium cross sections, they probe cross sections weighted with scattering angle, such as appear in the expression for nuclear viscosity. These appear reduced in lower-energy reactions by ~ 25 % compared to free space and the nuclear viscosity appears increased by a similar amount compared to that calculated with free cross sections.

The momentum-dependence of nucleonic mean fields at supranormal densities is best probed by momentum-dependence of elliptic flow in midperipheral collisions. The data favor a momentum dependence characterized by $m^*/m \sim 0.70$ at normal density, that strengthens as density increases in a similar manner to the DBHF calculations.

Most straightforward determination incompressibility is by analyzing the excitation of density oscillations. The far more precise measurements of giant monopole resonances than in the past suggest a value $K \sim 225$ MeV.

The flow in energetic reactions allows to place meaningful constraints on the nuclear pressure within the density range $2 \lesssim \rho/\rho_0 \lesssim 5$. The most extreme models for EOS can be eliminated.

REFERENCES

[1] E. Colin *et al.*, *Phys. Rev.* **C57**, R1032 (1998); R. Sun *et al.*, to be published.

[2] H.-J. Schulze *et al.*, *Phys. Rev.* **C55**, 3006 (1997); A. Schnell *et al.*, *Phys. Rev.* **C57**, 806 (1998).

[3] P. Danielewicz, *Phys. Lett.* **B146**, 168 (1984).

[4] W. Reisdorf *et al.*, *Nucl. Phys.* **A612**, 193 (1997).

[5] H. Feldmeier, J. Lindner, *Z. Phys.* **A341**, 83 (1991).

[6] S. Hama *et al.*, *Phys. Rev.* **C41**, 2737 (1990).

[7] P. Danielewicz, *Nucl. Phys.* **A673**, 375 (2000).

[8] L. Shi *et al.*, *Phys. Rev.* **C64**, 034601 (2001).

[9] D. Brill *et al.*, *Z. Phys.* **A355**, 61 (1996).

[10] G.Q. Li and R. Machleit, *Phys. Rev.* **C48**, 2707 (1993).

[11] C.-H. Lee *et al.*, *Phys. Lett.* **B412**, 235 (1997).

[12] D.H. Youngblood, *Nucl. Phys.* **A687**, 1c (2001).

[13] P. Danielewicz *et al.*, submitted for publication.